Journal of Molecular Liquids 351 (2022) 118575

Contents lists available at ScienceDirect

Journal of Molecular Liquids

journal homepage: www.elsevier.com/locate/molliq

Molecular dynamics investigations of ionic conductance at the nanoscale: Role of the water model and geometric parameters

Alia Mejri [a], Kamel Mazouzi [b], Guillaume Herlem [a], Fabien Picaud [a,b,*], Theo Hennequin [c], John Palmeri [d], Manoel Manghi [c]

[a] Laboratoire de Nanomédecine, Imagerie et Thérapeutiques, EA4662, UFR Sciences et Techniques, Centre Hospitalier Universitaire et Université de Bourgogne Franche Comté, 16 route de Gray, 25030 Besançon, France
[b] Mésocentre de calculs de Franche Comté, UFR Sciences et Techniques, Université de Bourgogne Franche Comté, 16 route de Gray, 25030 Besançon, France
[c] Laboratoire de Physique Théorique, Université de Toulouse, CNRS, UPS, 31062 Toulouse cedex 4, France
[d] Laboratoire Charles Coulomb (L2C), Université de Montpellier, CNRS, 34095 Montpellier cedex 5, France

ARTICLE INFO

Article history:
Received 15 November 2021
Revised 14 December 2021
Accepted 17 January 2022
Available online 24 January 2022

Keywords:
Molecular dynamic simulations
Confinement effect
Water models
Conductance

ABSTRACT

Ultra-efficient transport of water and ions at the nanoscale is studied through molecular dynamics simulations. Carbon nanotubes (CNTs) are used here as nanofluidic devices owing to their smooth inner structure and the compromise of a very simple composition for a tremendous variety of properties. Transport of solvated ions moving inside the carbon nanotube under the application of an external potential difference allowed the measurement of the ionic current established through the internal area of the tube. To be as exhaustive as possible, three popular water models were tested to investigate ionic transport inside this artificial nanochannel. The key geometric parameters of the carbon structure were also varied, revealing a peculiar dependence of the ionic conductance on each studied parameter in accordance with the theoretical model presented in this paper.

1. Introduction

The development of nanofluidics over the past decade has led to the acquisition of relevant data and the discovery of novel physical phenomena governing ion transport in confined spaces at nanoscale dimensions [1].

Such ion transport-based systems have opened up large opportunities for advanced nanofluidic devices in selective ion transport for engineering applications like desalination [2], water filtration [3], energy conversion [4,5] and harvesting [6,7], biosensors [8], biomimetic ion channels [9]. Furthermore, in the last few years, significant research advances have been made concerning the manufacture and development of nanoscale fluidic systems, both at the experimental and theoretical levels. A current challenge nowadays is to actively control and detect the motion of ions inside artificial nano-channels and to understand the mechanism governing this transport. It has also become essential to identify the influence of geometric parameters of the confining structure on fluid transport in narrow nano-channels.

Special attention has been paid to single walled carbon nanotubes (SWCNTs) as ideal conduction channels for fundamental nanofluidics studies, especially those related to water and ion transport. This is due to the simple composition of SWCNTs and their unique combination of properties: smooth walls, provided by their sp^2 carbon atoms hybridization, allowing fast motion of liquid and solvated ions with low fluid friction in addition to their remarkable chemical, mechanical, optical, and electronic properties. Moreover, their length can be controlled on the submicrometer to millimeter scale. Furthermore, depending on their crystal structure, the surface charge of carbon nanotubes can be actively controlled by an external electrical circuit [9]. In addition, the selectivity of CNTs towards transfering species (ions, for example) can be obtained by the targeting of well-defined sites at their entrance without affecting the interior walls of the structure [10,11]. CNTs can also mimic biological nanochannels as they share with them several structural motifs such as a narrow hydrophobic inner surface and local selective gates.

Activity around nanofluidics in ultra-confined environments has strongly risen through continuous progress in developing experimental tools. Many works have focused on the behavior of water and ions in carbon-based nanochannels. Lee et al. developed a novel method to produce high-quality CNT fibers by controlling

* Corresponding author at: Laboratoire de Nanomédecine, Imagerie et Thérapeutiques, EA4662, UFR Sciences et Techniques, Centre Hospitalier Universitaire et Université de Bourgogne Franche Comté, 16 route de Gray, 25030 Besançon, France.
E-mail address: fabien.picaud@univ-fcomte.fr (F. Picaud).

https://doi.org/10.1016/j.molliq.2022.118575
0167-7322/

the length of the water injection tube based on the feedstock decomposition temperatures [12].

Hassan et al. employed 2D 1H NMR to perform experimental measurements of water diffusion inside single and double walled CNTs. The measurements revealed a stratified fast diffusion for CNTs [13]. Moreover, previous experiments have demonstrated the possibility for a spontaneous filling of narrow CNTs with a diameter of the order of 2.7 Å [14]. Marcotte et al. highlighted a mechanically activated ionic transport inside 2-nm-radius multi-walled carbon nanotubes under the combination of mechanical and electrical forcing [15]. This study is in agreement with previous studies involving a mechanically activated excitatory ion current under mechanical pressure or stretching [16]. Several research groups are interested in the transport of water and ions inside carbon nanotubes and report in most situations linear I-V curves which are characteristic of an ohmic behavior. The conductivity values in these different studies could exceed the bulk conductivity by more than two orders of magnitude. Secchi et al. noted a conductance – concentration (G-C) variation suggesting that the conductance *G* with the salt concentration in the reservoirs, *C*, followed a power law behavior with exponent $\alpha = 1/3$ at low salt concentrations in individual CNTs of diameters in the tens of nanometer range. They attributed this tendency to an OH^- adsorption charge regulation mechanism at the surface of the carbon nanotube [17]. Yazda et al. have also confirmed this tendency for ionic current measurements through nanofluidic devices containing one or several SWCNTs of diameters ranging from 1.2 to 2 nm [18].

Several aspects of fluid transport CNTs have been rigorously explored basically by experiments employing electric field and pressure driven flows [19–21]. Despite the considerable advances in experimental studies [22], in particular during the last decade, the control of water and ion flow inside carbon nanotubes has not yet been established in the literature [23]. We therefore deemed it necessary to investigate further the novel properties of water in CNTs.

Theoretical and numerical approaches have now become of great interest in exploring the behavior of water inside carbon nanotubes. In particular, Molecular Dynamics (MD) allows achieving remarkable results with regard to the control and the description of water in a confined environment. Many studies discussed water permeability and ion selectivity in sub-nanometer carbon nanotubes revealing a peculiar water arrangement in strong confinement conditions related to the hydrogen bond network modification compared to the bulk water situation [24]. Different possible water arrangements were highlighted, ranging from single ordered chains in narrow CNTs to different ice tubes in wider CNTs [25–27]. Many other studies focused on the correlation between the geometrical characteristics of CNTs and the water flow. Besides, several studies have concluded that water flow inside single walled CNTs is metallicity and diameter dependent [28,29]. Thomas et al. [30] have conducted MD simulations for water motion in relatively narrow pores of diameters less than (or equal to) 1.6 nm, which may be suitable for desalination using reverse osmosis. They established that larger tube diameters lead to larger permeabilities of water inside the hydrophobic structure. Pascal et al. reported from MD simulations the entropy, enthalpy, and free energy of water confined in CNTs of diameters between 0.8 and 2.7 nm and highlighted a bulk-like liquid phase behavior for armchair tubes larger than 1.4 nm in diameter [31]. In addition, several works investigated the effect of grafting chemical functions on the dangling carbon atoms of the single walled SWCNTs. These chemical groups strongly enhance the performances of water desalination [30,32,33].

In the present work, we designed a nanofluidic system combining a single walled carbon nanotube with graphene sheets and studied the effect of geometry (tube diameter and length) of this hydrophobic pore on the ionic conductance of the system. We have simultaneously investigated three water models in order to generalize our approach and to select the most relevant one for the description of water and ion transport at the nanoscale.

2. System modeling and simulation methodology

The simulated nanopore is a single-walled carbon nanotube defined by Hamada (n,m) indices. The total nanofluidic device will be made of this CNT, with varying diameter, and length combined with two graphene sheets placed at its ends connecting two reservoirs of water and ions. In the current study we were not interested on the mechanical deformations of the CNT. The latter, as well as the graphitic edges of the reservoirs are taken as rigid structures. Each rectangular reservoir has the following dimensions (4.9,4.9,4.0) nm^3 and two openings are appropriately perforated in the two sheets to allow the solvent motion through the device and join the two symmetric regions of the simulation cell. In the first part of the current study we considered three armchair uncapped and uncharged CNTs with increasing diameters: (11,11), (13,13) and (15,15) CNTs of respectively 1.49, 1.76 and 2.03 nm. The electrolyte contains Na^+ and Cl^- ions at a concentration of 1 M in the reservoirs (see snapshot of the simulation in Fig. 1). All the simulations were performed using the NAMD 2.12 code [34]. MD simulations were conducted in the NPT ensemble with the pressure being maintained constant during the thermalization of the system. When an external electric field was applied the NVT ensemble was implemented, maintaining a constant volume throughout the simulation. The temperature was set to 300 K using Langevin dynamics. The particle mesh Ewald summation method (PME) [35] was used to calculate the full-system periodic electrostatic contributions. The integration time step was equal to 1 fs and the standard Charmm36 force field was used to describe force field and Lennard-Jones parameters for CNTs [36]. The water/CNT interaction was modeled using a Lennard-Jones 12-6 potential for all carbon atoms rather than the 9-3 Lennard-

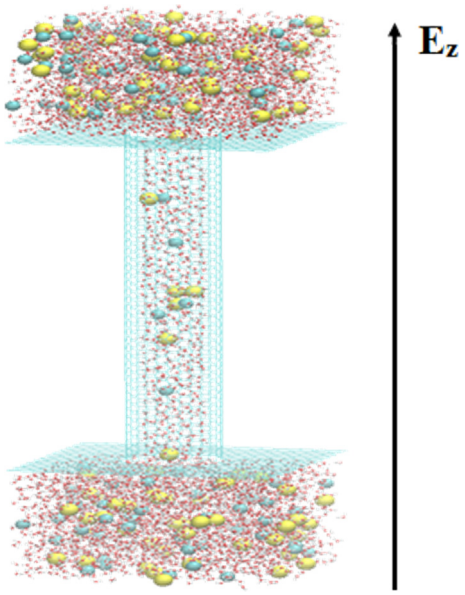

Fig. 1. Snapshot of the simulation system employed in the present study: (13,13) carbon nanotube combined with two graphene sheets is embedded in a periodic water box of 16,950 molecules. An external electric field is applied in the +z direction along the CNT axis.

Jones "featureless walls" potential. (a "featureless wall" approach is expected to break down for inter-wall separations below 1.6 nm [37]).

A set of three site rigid and non-polarizable water models were selected in order to evaluate the role of the water model on the ionic conductance of SWCNTs: TIP3P[38], SPC/E [39] and TIP4/2005 [40].

Different voltages (from 0.05 to 2 V) were applied to study the ionic current. For each simulation, 32,000 steps of minimization were first launched before running 5 ns of equilibration of the full system, the production runs were then performed for 30 ns at each voltage.

The TIP3P water model exhibits partial atomic charges centered on the hydrogen and oxygen atoms. It has a rigid geometry, which is consistent with water in the liquid phase. Moreover, TIP3P reasonably predicts the density and enthalpy of vaporization of water under ambient conditions [41]. The Charmm36 force fields were originally developed to study protein folding with the TIP3P water model [42]. A shortcoming of this model is that it overestimates the diffusion constant of water [43]. The SPC/E water model has also a rigid 3 site structure with different partial charges. This model does not reproduce the experimental geometry of a water molecule in the gas phase. It uses only two values for bond length and bond angle (see Table 1). It was established in the literature that SPC/E accurately predicts the diffusion of water at ambient conditions and reproduces well the dielectric properties of water at 298 K. The last water model tested in the current study is the TIP4P/2005. This model is a 4 site rigid water model which shifts the negative partial charge from the oxygen atom towards a virtual site located along the bisector of the HOH angle. This model is interesting as it provides a good description of many water properties. In particular, it leads to a good agreement between theoretical and experimental diffusion coefficient values in the low temperature range, including room temperature (300 K) for which it was designed [43].

The three water models are considered as non-polarizable and the geometry of each water model is given in Fig. 2. The pair potential between the water molecules has the following form (Eq. 1):

$$\upsilon = 4\varepsilon\left[\left(\frac{\sigma}{r_{oo}}\right)^{12} - \left(\frac{\sigma}{r_{oo}}\right)^{6}\right] + \sum_{i,j\in w}\frac{q_i q_j}{r_{ij}} \quad (1)$$

where σ and ε are the Lennard-Jones (LJ) parameters between oxygen atoms and q_i the charge on i^{th} site of water. The values of these parameters are given in Table 1. r_{ij} is the distance between the sites i and j in the different water molecules.

3. Results and discussion

3.1. Role of the CNT diameter on the ionic conductance

MD simulations were first conducted on CNTs with different diameters for all water models in order to understand the role of this geometric parameter on the conductance values. Theoretical I = f (V) curves for the three diameters and for each water model are plotted in Fig. 3. Five voltages were used, ranging from 0.5 to 2 V. As can be seen in Fig. 3, the diameter increase did not modify the curve shape but only its slope, whatever the water model used in the simulations. The linear curve fit allowed us to estimate the conductance values of these CNTs in all situations. The results are summarized in Table 2.

The conductance values keep, whatever the model, the same variation trend. In fact, for increasing diameters and for the same chirality, the conductance of the system increases as the diameter of the tube increases. The obtained values of conductance fall within the range of the experimental data with corresponding diameters [44,45]. Indeed, in these studies, the conductance varies with pH and ionic concentration with values ranging from 0.4 to 1.5 nS.

This increase of conductance is in agreement with theoretical modeling of conductance in nanopores. For small neutral pores, the electrical resistance is the sum of the constant access resistance and the pore one. Hence the full nanopore conductance (Eq. 2) as a function of the pore radius R and the pore length L is for a neutral pore [46]

$$G(R,L) = \frac{\pi(R-R_{vdw})^2}{L}\frac{e^2(\mu_+ + \mu_-)c_{pore}}{1+\frac{\pi}{2}\frac{R-R_{vdw}}{L}} \quad (2)$$

where R_{vdw} is the van der Waals radius associated with the hydrophobicity of the CNT, e is the electron charge, $\mu_\pm$ are the ionic mobilities, and c_{pore} the ionic concentration in the pore. The corrective factor $\frac{1}{1+\frac{\pi}{2}\frac{R-R_{vdw}}{L}}$ to the nanopore conductance comes from the presence of the access resistance due to the small length of the CNTs studied. [47] By fitting the data for the conductance as a function of the pore diameter for $L = 10$ nm, and taking $R_{vdw} = 0.3$ nm as extracted from the water radial density distribution shown in Fig. 5, one obtains a reasonable fit, shown in Fig. 4 with $c_{pore} \approx 0.49$ M for $\mu_+ = 3.9 \times 10^{11}$ s/kg for $Na^{\pm}$ and $\mu_- = 5.4 \times 10^{11}$ s/kg for Cl^- [48] (and $c_{pore} \approx 0.37$ M for $\mu_+ = 5.6 \times 10^{11}$ s/kg for $Na^{\pm}$ and $\mu_- = 7.1 \times 10^{11}$ s/kg for Cl^- [49]). Note that we fitted the 2 last points corresponding to the larger radii. By fitting the 4 points we obtain slightly smaller values for the concentration (orange curves).

Table 1
(a) The force field parameters of SPC/E, TIP4P, and TIP4P/2005. (b) Experimental and simulation data of different water models. Thermodynamic conditions as reported in each entry.

(a)

Molecular Model	TIP3P	SPC/E	TIP4P/2005	SWCNT
σ (Å)	3.1506	3.1660	3.1589	3.3997
ε (kJ/mol)	0.6364	0.6500	0.7749	0.3598

(b)

Parameter	TIP3P	SPC/E	TIP4P/2005	Exp
D self-diffusion Coefficient ($\times 10^{-9}$ $m^2.s^{-1}$)	5.65	2.5	2.08/2.39	2.3
ΔH_{vap} (kcal/mol)	10.5	11.79	11.99	10.52
ε(298 K)	94–100	71.8	59–63	78.6
ρ_{298k} (g/cm^3)	0.98	0.994	0.993	0.997
$gOO_{1,2}$	2.77, 4.50	2.75, 4.50	2.43, 4.38	2.88, 4.50
gOH	1.83	1.77	–	1.85

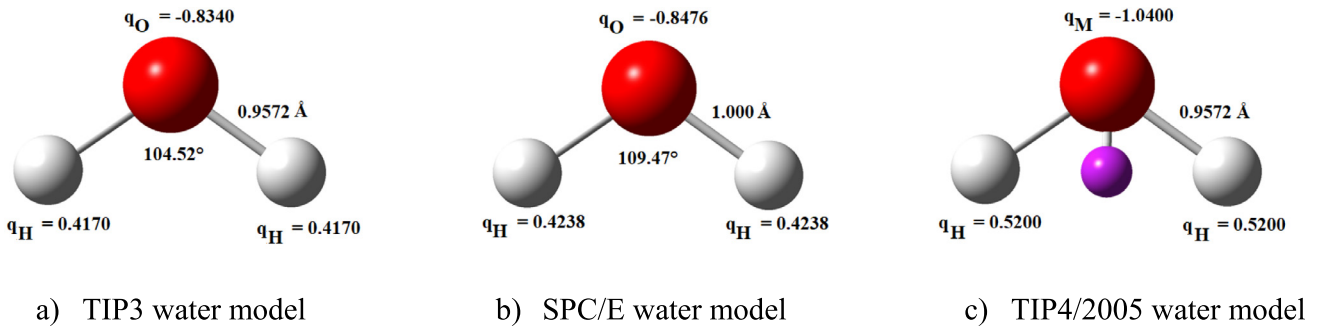

Fig. 2. Representation of TIP3P, SPC/E and TIP4P/2005 geometries. Oxygen atoms are shown in red, hydrogen atoms in white and the TIP4P/2005 virtual site is in purple.

Interestingly, this fitted pore concentration is smaller than the reservoir concentration of $c_b = 1$ M, which is the signature of a transfer free-energy penalty (or Potential of Mean Force, PMF) on the order of $W = -k_B T \ln\left(\frac{c_{pore}}{c_b}\right) \approx 0.8 k_B T$. This free-energy penalty might be due to dielectric exclusion [50], Born exclusion [51] and solvation deficit [52].

The hydrodynamic fluid (of viscosity η) velocity profile in the nanopore $v(r)$ (where r is the radial distance) including fluid slippage at the surface, with a slip length b, is given by the modified Helmholtz-Smoluchowski equation (Eq. 3)

$$v(r) = \frac{\epsilon_0 \epsilon}{\eta}[\phi(R) - \phi(r)]E - \frac{1}{4\eta}\partial_z p(R^2 - r^2) - \frac{b}{\eta}\left(\sigma E + \frac{R}{2}\partial_z p\right) \quad (3)$$

where E and $\partial_z p$ are the applied electric field and pressure gradient ($\phi(r)$ is the electrostatic potential and σ the surface charge density) (see Appendix of [46]. The last term corresponds to the slip velocity. Its contribution to the ionic current is $I = 2\pi \int_0^R \rho_c(r) v(r) r dr$ where $\rho_c(r)$ is the ionic charge density. For neutral pores, fluid slippage would therefore only appear if the pressure gradient and the ionic charge density in the pore were non-zero. Hence in the present case of neutral pores, we expect that it does not play any role in the conductance. For charged pores with surface charge density σ, however, it has been shown that fluid slippage increases the conductance with an additional contribution equal to $G_{slip} = 2\pi \frac{Rb}{\eta L}\sigma^2$ [46].

In addition, we notice that the three models do not behave in the same way with respect to the conductance values. Indeed, the conductance values for the SPC/E and TIP4P/2005 are reduced compared to the TIP3P water model. In order to understand the differences between the water models, it is important to observe the structure of the water inside the carbon cage. We show in Fig. 5 snapshots of water arrangement viewed on top of the system made of the (13,13) CNT for the three water models. It is very difficult to demonstrate using these different snapshots the role played by the models in the calculated conductance values. In Fig. 6 we therefore plot the radial density distribution of water oxygen atoms towards carbon atoms of the tube within the (13,13) armchair CNT.

It should be noted that in the three situations (differing only by the water model) we observed a particular arrangement of water molecules in the confined state. Two specific average positions are occupied by the oxygen atoms at 4 Å and 7 Å from the pore wall, respectively. These peaks appear because the water molecules adopt a circular ring structure when they are encapsulated inside cylindrical structures such as CNTs. This structure is often noted in the literature [53] and is due to the hydrophobic properties of the carbon wall. Several numerical and experimental studies have shown that confined water in thin pores is highly structured and tends to arrange itself into a tubular structure composed of wet layers made of water channel molecules with a single file of water molecules located near the pore center [54–58]. Moreover, we observe a cylindrical volume of width 0.3 nm which is free of water molecules for the three models. It corresponds to a vacuum zone that arises due to the hydrophobicity of the carbon wall.

The three water models seem, however, to exhibit the same behavior towards the carbon cage. The water behavior toward the inner pore surface of the tube could thus not explain the different conductance value obtained for TIP3P water. The radial density distributions of water oxygen atoms towards the carbon structure (Fig. 6) present the same position for all the peaks. Note also that this behavior is also preserved for the two other pore diameters considered in this study (plots are provided in the supplementary information Section S2). The only differences come from the heights of the peaks. TIP4P/2005 model is the only one that presents a clearly different radial density distribution behavior, even though it presents the same conductance values as the SPC/E one. We cannot therefore explain the different conductance values by the behavior of the water molecules near the surface of the carbon cage.

To investigate water molecule structures inside CNT and attempt to explain the conductance values, we calculated the average number of hydrogen bonds per water molecule for water in the bulk and confined in the CNT (Table 3). Additionally, the radial distribution functions between oxygen atoms in the confined situations were also plotted in Fig. 7.

Hydrogen bond number gives information about water arrangement within the tube for each model. As shown in Table 3, the modifications of this H-bond number are not significant in CNT (13,13), even though the conductance values can increase by a factor of two between TIP3P model and the other two water models (see Table 1). Moreover, the radial density distributions shown in Fig. 7 clearly indicate a slight shift of the first distribution peak, related to the water models adopted here. This confirms that internal water molecule arrangement depends on the model, although the three models presented a similar behavior with respect to the external carbon cage.

Based on these data, we conclude that SPC/E and TIP4P/2005 water models are more structured in a confined medium than the TIP3P model. This will probably impact the ion pore entry rates and thus the conductance values obtained for our different simulated systems under the same conditions. This is in accordance with previous theoretical studies made by Liu et al. [59–61].

Several studies have also found different behaviors for these 3 water models based on MD simulations and transport properties such as self-diffusion coefficients D, shear viscosities η and thermal conductivities λ. Among them, Hi et al. have employed the Green-Kubo relations to calculate the transport properties of SPC/E and TIP4P/2005 water over a range of temperatures from 243 to 550 K. They obtained the best agreement with the experimental value of D for the TIP4P/2005 water model at low temperatures (including 300 K). Also the shear viscosity for TIP4P/2005 water

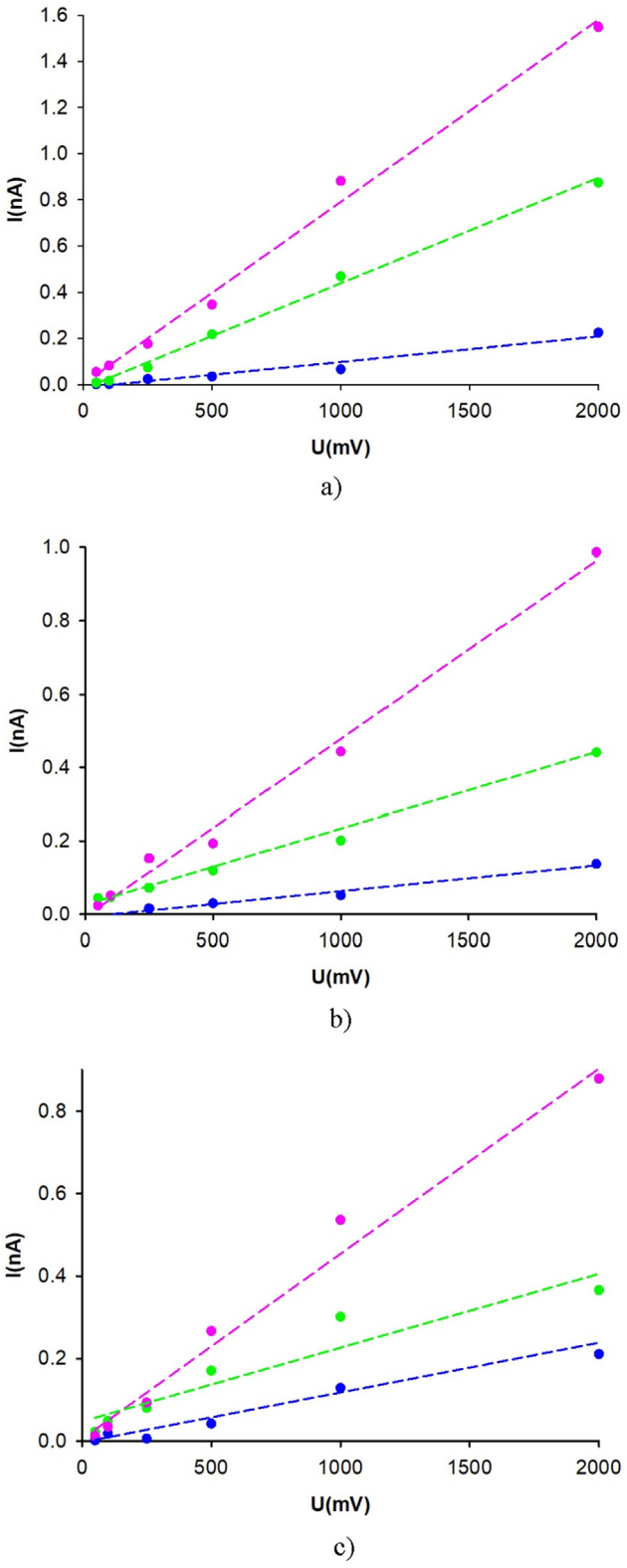

Fig. 3. Simulation results (data points) and theoretical curves for I = f(U) for the 3 water models used in our simulations. Blue, green and pink dashed curves represent the (11,11), (13,13) and (15,15) CNTs, respectively. Results obtained for (a) TIP3P, (b) SPC/E and (c) TIP4P/2005 models, respectively.

model shows less deviation from the experimental data [62]. Celebi et al. compared, among other properties, the slip length of water on rigid graphene nanochannels. This quantity is strongly

Table 2
Conductance values for different tube diameters and different water models.

Water model	Hamada indices (n, m)	Diameter d (nm)	Conductance G (nS)
TIP3P	(11,11)	1.485	0.11 ± 0.06
	(13,13)	1.755	0.46 ± 0.06
	(15,15)	2.025	0.79 ± 0.03
SPC/E	(11,11)	1.485	0.070 ± 0.005
	(13,13)	1.755	0.21 ± 0.08
	(15,15)	2.025	0.49 ± 0.04
TIP4P/2005	(11,11)	1.485	0.11 ± 0.03
	(13,13)	1.755	0.18 ± 0.03
	(15,15)	2.025	0.46 ± 0.04

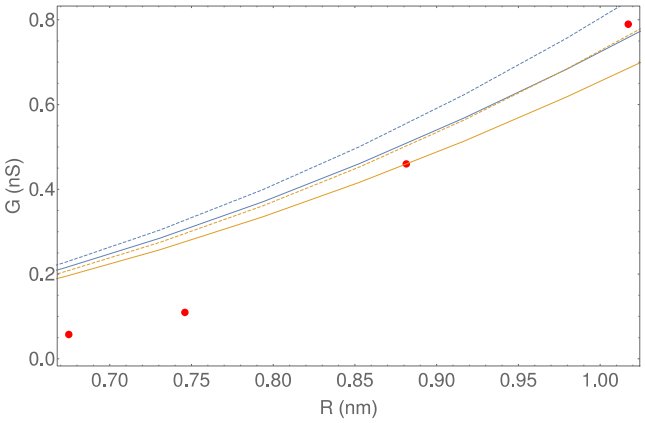

Fig. 4. Fit of the conductance simulation data (red dots) for CNTs of length L = 10 nm and various radii with the TIP3P water model. The blue (respectively orange) curve corresponds to a fit of the two last (reps. four) points. The dashed curves correspond to the case without access resistance.

sensitive to the choice of the water model (specifically its shear viscosity). They concluded that TIP4P/2005 gives the best prediction of viscosity, within 1.7% of the experimental value. SPC/E model is also moderately accurate, while TIP3P model shows poorer performance in reproducing the experimental viscosity at specified thermodynamic conditions [63]. Losey et al. [64] evaluated, by force driven flow, the performance of different water models through water flow calculations within CNTs of increasing diameter separating dual reservoirs. They observed in all simulations the highest pore water flow for TIP3P water model compared to the TIP4P/2005 and SPC/E ones, which behave similarly. They correlated their results to the shear viscosity of each model, in accordance with those of other research groups [43,65,66].

Therefore, our results show a stronger organization of water molecules in the SPC/E and TIP4P/2005 models. This modification impacts necessarily the physical observables measured in nanofluidic simulations. As a consequence, we can arrive at the same conclusion for the TIP3P model since the conductance of the CNT is already impacted when using this model. The higher water flow in the TIP3P model compared to the SPC/E and TIP4P/2005 ones due to its larger bulk diffusion constant, is thus an overestimation for CNTs. Therefore, we conclude that the SPC/E and TIP4P/2005 models should be the most appropriate models for nanofluidic studies [60,61,67].

Ionic organization inside nanopore:

Ionic distribution inside a CNT is an interesting indicator that can be used to account for the differences between the three water models tested in our simulations. Fig. 8 shows the distribution of sodium and chloride ions as well as water molecules inside the (13,13) tube of intermediate diameter. Two important conclusions

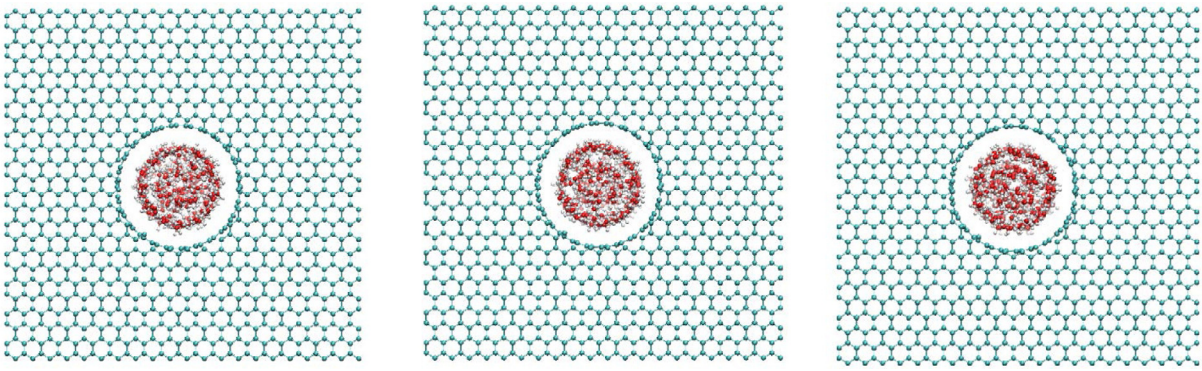

Fig. 5. Top views of the water confined in the (13,13) armchair carbon nanotube for: (a) TIP3P (b) SPC/E and (c) TIP4P/2005 water models.

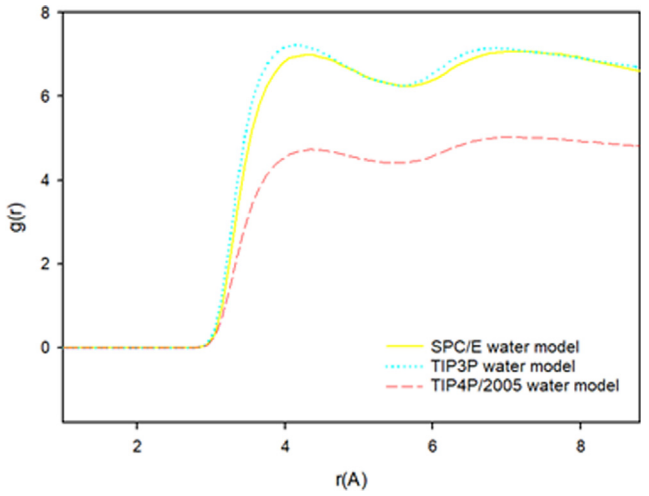

Fig. 6. Radial density distribution of water oxygen atoms towards carbon atoms within (13,13) CNT (cyan dotted points, yellow and red dotted curves represent TIP3P, SPC/E and TIP4P/2005 water models).

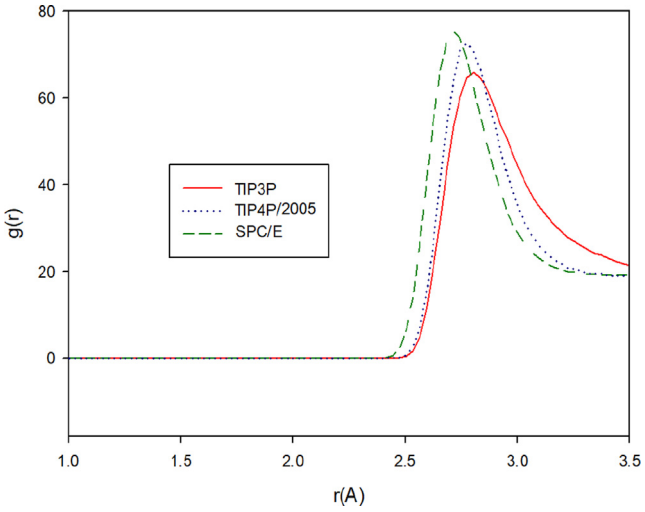

Fig. 7. Radial density distribution of water oxygen atoms within (13,13) CNT (green, blue and red dotted curves represent SPC/E, TIP4P/2005 and TIP3P water models, respectively).

Table 3
Average number of hydrogen bonds per water molecule for water in bulk and within the (13,13) CNT.

Model	Average in bulk	Average in CNT
TIP3P	1.00 (0.015)	1.00 (0.035)
SPC/E	1.27 (0.015)	1.27 (0.035)
TIP4P/2005	1.04 (0.02)	1.05 (0.03)

can be reached. Whatever the model, the ionic distribution is always located at the same position with respect to the water molecules distribution. The different peaks are almost situated at the same abscisses. Water molecules are organized appreciably identically with respect to the tube internal surface.

It should also be noted that the ions generally have a preferential circulation region inside the carbon nanotube. In accordance with the peaks related to each ion, sodium ions move in two specific regions located at the center of the tube (in majority), as well as at the limit of the second water tube created inside the carbon cage. Chloride ions move only in the zone of the CNT located between the cation localizations to maintain the overall electroneutrality of the system. Their trajectory remains offset from the center of the tube which is the region of a continuous movement of the sodium ions. The higher number of cation peaks reflects better organization of the water with respect to these ions and therefore better stability of the latter within the host structure. Indeed, the first peak of cations is well defined between the two water peaks. Sodium ions are therefore clearly better solvated than the anions (Cl^-).

Effect of pore length on the CNT conductance

We have investigated the role of the pore length increase on the ionic conductance. In these simulations four lengths were tested for uncapped and uncharged (13,13) CNT. All simulations were performed for a constant potential of 1 V.

We plotted in Fig. 9, the CNT conductance variation as a function of the tube length. As observed for the other parameters, the conductance presents the same qualitative behavior for the three water models, but with a different amplitude. Indeed, when the tube length increases, the conductance shows a marked decrease for the TIP3P model and a smaller one for the SPC/E model.

Note that we have widened the range of lengths up to 80 nm for the smallest tube ((10,10) with d = 1.34 nm). This was possible due to the size of the system which remained reasonable in this specific case. The conductance shows a small increase at small lengths before a strong decrease until the maximal length used in the simulations for which we reached the value of 0.017 nS (see S5 in sup-

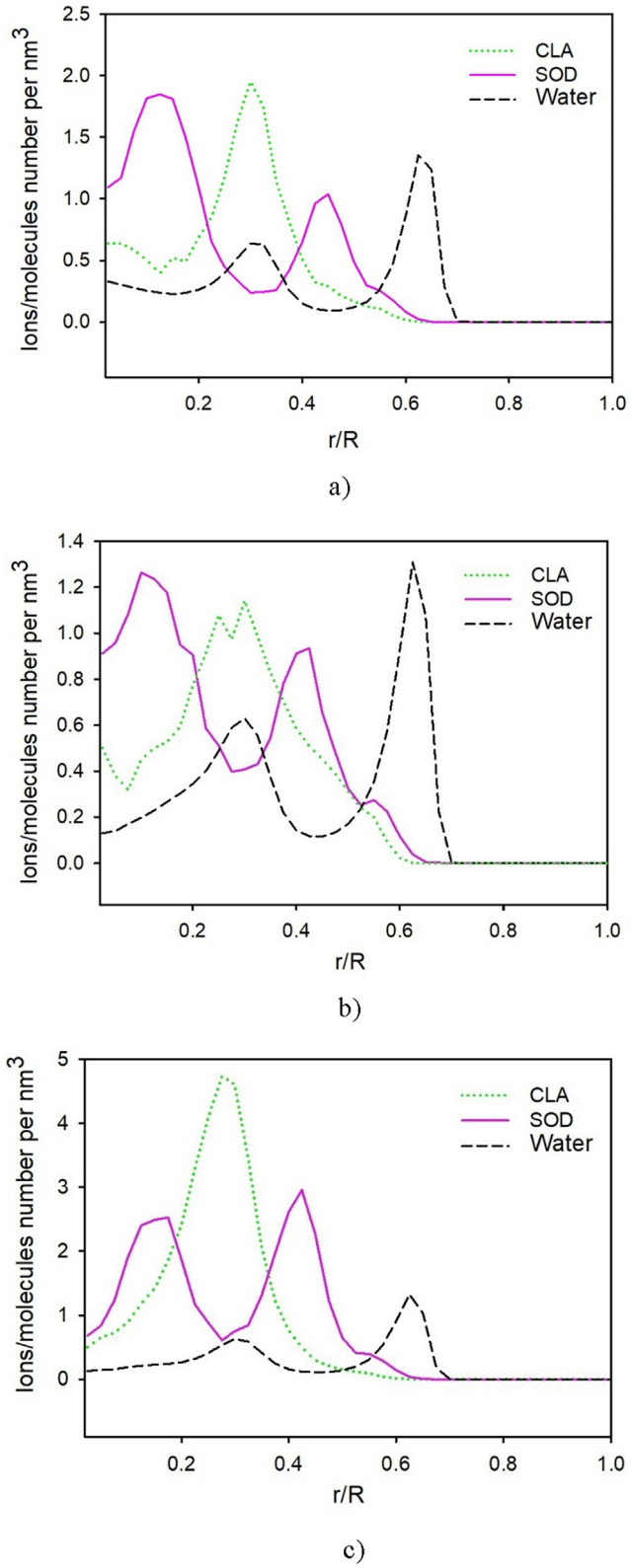

Fig. 8. Water and ions distribution inside (13,13) CNT (Cl^- ions are in green dotted lines; Na^+ in pink and water in black dashed lines). Results obtained for (a) TIP3P, (b) SPC/E and (c) TIP4P/2005 models, respectively.

plementary Information's section). To complete this analysis, we computed the ionic concentration values inside each studied CNT as a function of the water model.

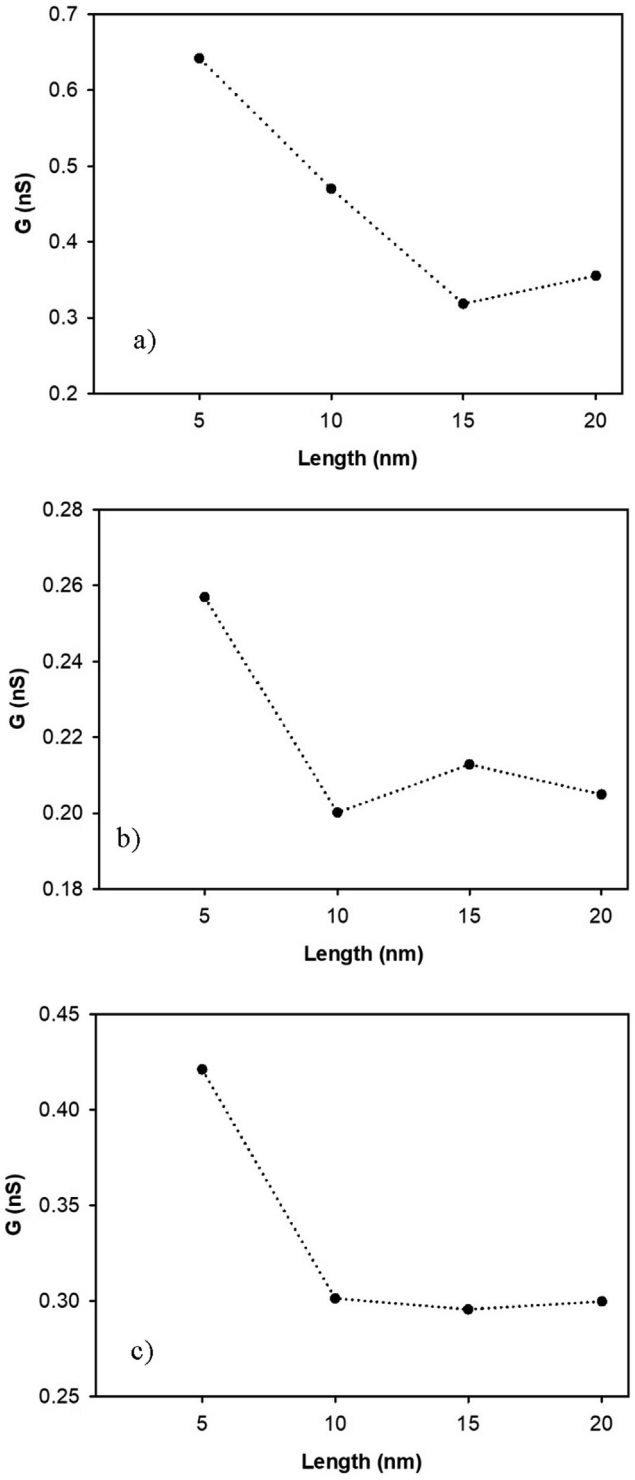

Fig. 9. CNT conductance as a function of the uncharged (13,13) CNT pore length. Results obtained for (a) TIP3P, (b) SPC/E and (c) TIP4P/2005 models, respectively.

As shown in Table 4, in the major part of the simulations, the ionic concentrations inside the CNTs (even for the highest tube diameter) did not reach the concentration in the reservoir bulk ($c_{bulk} = 1$ M). Furthermore, fitting the data for TIP3P a shown in Fig. 10 with Eq. (1) leads to $c_{pore} \approx 0.25$ M for the (10,10) and $c_{pore} \approx 0.29$ for the (13,13) CNT, in agreement with the measured concentration in the pore of 0.3 M.

Table 4
Ionic concentration in mol/L calculated inside the different CNTs for each water model. The accessible volume used to estimate these concentrations is computed with a water occupation diameter d^* inside the CNT, i.e. $d^* = d_{CNT} - 0.6$ (in nm). For the smallest tube radius tested in this article ((10,10) CNT) with the TIP3P water model, the inner ion concentration was equal to 0.35 M.

	(11,11)	(13,13)	(15,15)
TIP3P	0,22 ± 0.06	0,3 ± 0.1	0,7 ± 0.1
SPC/E	0,31 ± 0.08	0,55 ± 0.07	0,74 ± 0.07
TIP4P/2005	1,01 ± 0.07	1,1 ± 0.1	1,1 ± 0.1

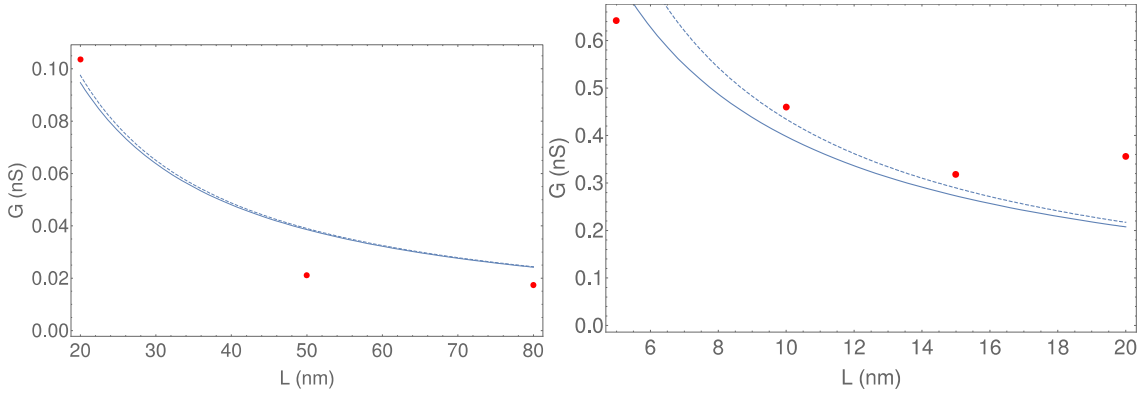

Fig. 10. Fit of the conductance simulation data (red dots) for the (10,10) (left) and (13,13) (right) CNTs vs. their length L with the TIP3P water model. Blue solid curves correspond to a fit with Eq. (1), dashed ones corresponds to the case without access resistance.

It thus confirms the validity of Eq. (1) and a PMF of $W = -k_BTln(c_{pore}/c_b) \approx 1.2k_BT$ for the (13,13) CNT with the TIP3P water model.

The decrease of the conductance with the length L is semi-quantitatively described by Eq. (1), with a constant access resistance in series with a pore resistance which increases linearly with L. The slight increase of the conductance observed for $L < 20$ nm in the (10,10) case is however not captured by Eq. (1) and might be due to specific hydration effects for small CNT radii. The role of the graphene sheets located at the extremities of the CNT can also explain this behavior by reinforcing the access resistance. Hence, for small tube length values, there subsists a strong competition between the 2 resistance contributions while one takes predominance as soon as the tube length increases.

4. Conclusions

In this work, we have studied through MD simulations the electric field-driven electrolyte transport through CNTs. We focused on the effect of the geometrical parameters of single-walled carbon nanotubes, such as diameter, length and helicity, on the ionic conductance of the system. Three popular water models were investigated, namely TIP3P, SPC/E and TIP4P/2005. Several key results were reported: (i) The increase in the CNT diameter tends to increase the value of the conductance. (ii) The increase of the tube length involves a decrease of the conductance values (more or less strong depending on the water model). These results have been nicely interpreted by our theoretical model where the access resistance and the pore one act in series. In particular, we show that the ionic partition coefficient $\frac{c_{pore}}{c_b}$ is less than one for neutral CNTs, which we interpret as resulting from dielectric exclusion and possibly a hydration deficit of ions in the CNT.

An important part of this work was dedicated to the study of different water models in order to find the most adequate ones for a physically appropriate description of water and ion transport at the nanoscale. Our numerical simulations allowed us to conclude that: (i) The water model has no effect on the conductance trend with increasing tube diameter, it only impacts the conductance values. (ii) Hydrogen bond analysis gives information on water arrangement within the pore and SPC/E and TIP4P/2005 models behave in the same way. They are much more structured than the TIP3P model, which explains the different values obtained for the conductances. iii) Computational cost of the three models for the (13,13) tube, shows that, the four-center model TIP4P/2005 requires a computational time 30% greater than the two other three-center models. In addition, the TIP3P model overestimates the water diffusion coefficient resulting in conductance values twice those obtained for the two other models. The good compromise between the different results obtained in this work along with the computational cost suggest that the SPC/E and TIP4P/2005 water models should be best suited for the study of water inside carbon nanotubes.

CRediT authorship contribution statement

Alia Mejri: Conceptualization, Methodology, Writing. **Kamel Mazouzi:** Conceptualization, Methodology. **Guillaume Herlem:** Conceptualization, Writing – review & editing. **Fabien Picaud:** Conceptualization, Methodology, Supervision, Writing – review & editing. **Theo Hennequin:** Conceptualization, Methodology, Writing – review & editing. **John Palmeri:** Conceptualization, Methodology, Writing – review & editing. **Manoel Manghi:** Conceptualization, Methodology, Supervision, Writing – review & editing.

Declaration of Competing Interest

The authors declare that they have no known competing financial interests or personal relationships that could have appeared to influence the work reported in this paper.

Acknowledgments

Author contributions: Conceptualization and methodology, A.M., G. H., K.M., M.M, T. H, J.P. and F.P.; simulation, A.M.; writing, A.M, G.

H., M.M, T. H, J.P. and F.P. All authors have read and agreed to the published version of the manuscript.

Funding

This work was funded by Agence Nationale de la Recherche (ANR-18-CE09-0011-01"IONESCO"). Calculations were performed at the supercomputer regional facility Mesocentre of the University of Franche-Comté.

Data availability statement

Data available on demand.

Appendix A. Supplementary material

Supplementary data to this article can be found online at https://doi.org/10.1016/j.molliq.2022.118575.

References

[1] L. Bocquet, Nanofluidics coming of age, Nat. Mater. 19 (3) (2020) 254–256.
[2] C.H. Ahn, Y. Baek, C. Lee, S.O. Kim, S. Kim, S. Lee, S.-H. Kim, S.S. Bae, J. Park, J. Yoon, Carbon nanotube-based membranes: fabrication and application to desalination, J. Ind. Eng. Chem. 18 (5) (2012) 1551–1559.
[3] M. Fasano, T. Humplik, A. Bevilacqua, M. Tsapatsis, E. Chiavazzo, E.N. Wang, P. Asinari, Interplay between hydrophilicity and surface barriers on water transport in zeolite membranes, Nat. Commun. 7 (2016) 12762.
[4] K. Xiao, L. Jiang, M. Antonietti, Ion transport in nanofluidic devices for energy harvesting, Joule 3 (10) (2019) 2364–2380.
[5] K. Xiao, P. Giusto, L. Wen, L. Jiang, M. Antonietti, Nanofluidic ion transport and energy conversion through ultrathin free-standing polymeric carbon nitride membranes, Angew. Chem. Int. Ed. 57 (32) (2018) 10123–10126.
[6] Z. Zhang, X. Li, J. Yin, Y. Xu, W. Fei, M. Xue, Q. Wang, J. Zhou, W. Guo, Emerging hydrovoltaic technology, Nat. Nanotechnol. 13 (2018) 1109–1119.
[7] A. Siria, P. Poncharal, A.L. Biance, R. Fulcrand, X. Blase, S.T. Purcell, L. Bocquet, Giant osmotic energy conversion measured in a single transmembrane boron nitride nanotube, Nature 494 (2013) 455–458.
[8] J. Guoa, J. He, B. Zenga, Carbon nanotube based nanopore and nanofluidic devices towards biosensing.
[9] H. Amiri, K.L. Shepard, C. Nuckolls, R. Hernández Sánchez, Single-walled carbon nanotubes: mimics of biological ion channels, Nano Lett. 17 (2017) 1204–1211.
[10] J. Geng, K. Kim, J. Zhang, A. Escalada, R. Tunuguntla, L.R. Comolli, F.I. Allen, A.V. Shnyrova, K.R. Cho, D. Munoz, Y.M. Wang, C.P. Grigoropoulos, C.M. Ajo-Franklin, V.A. Frolov, A. Noy, Stochastic transport through carbon nanotubes in lipid bilayers and live cell membranes, Nature 514 (2014) 612–615.
[11] R. Tao, X. Gao, D. Lin, Y. Chen, Y. Jin, X. Chen, S. Yao, P. Huang, J. Zhang, Z. Li, The role of entrance functionalization in carbon nanotube-based nanofluidic systems: an intrinsic challenge, Phys. Fluids 33 (1) (2021) 012015, https://doi.org/10.1063/5.0037208.
[12] S.-H. Lee, J. Park, H.-R. Kim, J. Lee, K.-H. Lee, Synthesis of high-quality carbon nanotube fibers by controlling the effects of sulfur on the catalyst agglomeration during the direct spinning process, RSC Adv. 5 (52) (2015) 41894–41900.
[13] J. Hassan, G. Diamantopoulos, L. Gkoura, M. Karagianni, S. Alhassan, S.V. Kumar, M.S. Katsiotis, T. Karagiannis, M. Fardis, N. Panopoulos, H.J. Kim, M. Beazi-Katsioti, G. Papavassiliou, Ultrafast stratified diffusion of water inside carbon nanotubes; direct experimental evidence with 2D D-T2 NMR spectroscopy, J. Phys. Chem. C 122 (19) (2018) 10600–10606.
[14] S. Cambré, B. Schoeters, S. Luyckx, E. Goovaerts, W. Wenseleers, Experimental observation of single-file water filling of thin single-wall carbon nanotubes down to chiral index (5,3), Phys. Rev. Lett. 104 (20) (2010), https://doi.org/10.1103/PhysRevLett.104.207401.
[15] A. Marcotte, T. Mouterde, A. Niguès, A. Siria, L. Bocquet, Mechanically activated ionic transport across single-digit carbon nanotubes, Nat. Mater. 19 (10) (2020) 1057–1061.
[16] C.D. Cox, N. Bavi, B. Martinac, Biophysical principles of ion-channel-mediated mechanosensory transduction, Cell Rep. 29 (1) (2019) 1–12.
[17] E. Secchi, A. Niguès, L. Jubin, A. Siria, L. Bocquet, Scaling behavior for ionic transport and its fluctuations in individual carbon nanotubes, Phys. Rev. Lett. 116 (15) (2016), https://doi.org/10.1103/PhysRevLett.116.154501.
[18] K. Yazda, S. Tahir, T. Michel, B. Loubet, M. Manghi, J. Bentin, F. Picaud, J. Palmeri, F. Henn, V. Jourdain, Voltage-activated transport of ions through single-walled carbon nanotubes, Nanoscale 9 (33) (2017) 11976–11986.
[19] R.J. Castellano, R.F. Praino, E.R. Meshot, C. Chen, F. Fornasiero, J.W. Shan, Scalable electric-field-assisted fabrication of vertically aligned carbon nanotube membranes with flow enhancement, Carbon 157 (2020) 208–216.
[20] D. Toghraie, M. Hekmatifar, Y. Salehipour, M. Afrand, Molecular dynamics simulation of Couette and Poiseuille Water-Copper nanofluid flows in rough and smooth nanochannels with different roughness configurations, Chem. Phys. 527 (2019) 110505, https://doi.org/10.1016/j.chemphys.2019.110505.
[21] T. Yoshioka, R. Kunimori, I. Hisaoka, H. Nagasawa, M. Kanezashi, T. Tsuru, Molecular dynamics simulation study on the mechanisms of liquid-phase permeation in nanopores, Sep. Purif. Technol. 220 (2019) 259–267.
[22] K. Ritos, M.K. Borg, N.J. Mottram, J.M. Reese, Electric fields can control the transport of water in carbon nanotubes, Philos. Trans. Royal Soc. A: Math. Phys. Eng. Sci. 374 (2060) (2016) 20150025, https://doi.org/10.1098/rsta.2015.0025.
[23] K. Xiao, L. Chen, L. Jiang, M. Antonietti, Carbon nitride nanotube for ion transport based photo-rechargeable electric energy storage, Nano Energy 67 (2020) 104230.
[24] Q. Chen, Q. Wang, Y.-C. Liu, T. Wu, The effect of hydrogen bonds on diffusion mechanism of water inside single-walled carbon nanotubes, J. Chem. Phys. 140 (2014) 214507.
[25] H. Kumar, C. Dasgupta, P.K. Maiti, Structure, dynamics and thermodynamics of single-file water under confinement: effects of polarizability of water molecules, RSC Adv. 5 (2015) 1893–1901.
[26] S. Chakraborty, H. Kumar, C. Dasgupta, P.K. Maiti, Confined water: structure, dynamics, and thermodynamics, Acc. Chem. Res. 50 (9) (2017) 2139–2146.
[27] Y. Jia, X. Lu, Z. Cao, T. Yan, From a bulk to nanoconfined water chain: bridge water at the pore of the (6,6) carbon nanotube, PCCP 22 (2020) 25747–25759.
[28] A. Panahi, P. Sadeghi, A. Akhlaghi, M.H. Sabour, Investigating the effect of single-walled carbon nanotubes chirality on the electrokinetics transport of water and ions: a molecular dynamics study, Diam. Relat. Mater. 110 (2020) 108105, https://doi.org/10.1016/j.diamond.2020.108105.
[29] A. Sam, V. Prasad, S.P. Sathian, Water flow in carbon nanotubes: the role of tube chirality, physical chemistry chemical physics, PCCP 21 (12) (2019) 6566–6573.
[30] M. Thomas, B. Corry, A computational assessment of the permeability and salt rejection of carbon nanotube membranes and their application to water desalination, Philos. Trans. Royal Soc. A: Math. Phys. Eng. Sci. 374 (2016) 20150020.
[31] T.A. Pascal, W.A. Goddard, Y. Jung, Entropy and the driving force for the filling of carbon nanotubes with water, Proc. Natl. Acad. Sci. 108 (2011) 11794–11798.
[32] W. Chen, S. Chen, T. Liang, Q. Zhang, Z. Fan, H. Yin, K.-W. Huang, X. Zhang, Z. Lai, P. Sheng, High-flux water desalination with interfacial salt sieving effect in nanoporous carbon composite membranes, Nat. Nanotechnol. 13 (2018) 345–350.
[33] A. Chogani, A. Moosavi, A. Bagheri Sarvestani, M. Shariat, The effect of chemical functional groups and salt concentration on performance of single-layer graphene membrane in water desalination process: a molecular dynamics simulation study, J. Mol. Liq. 301 (2020) 112478, https://doi.org/10.1016/j.molliq.2020.112478.
[34] J.C. Phillips, R. Braun, W. Wang, J. Gumbart, E. Tajkhorshid, E. Villa, C. Chipot, R. D. Skeel, L. Kalé, K. Schulten, Scalable molecular dynamics with NAMD, J. Comput. Chem. 26 (2005) 1781–1802.
[35] T. Darden, D. York, L. Pedersen, Particle mesh Ewald: an N·log(N) method for Ewald sums in large systems, J. Chem. Phys. 98 (1993) 10089–10092.
[36] A.D. MacKerell, D. Bashford, M. Bellott, R.L. Dunbrack, J.D. Evanseck, M.J. Field, S. Fischer, J. Gao, H. Guo, S. Ha, D. Joseph-McCarthy, L. Kuchnir, K. Kuczera, F.T. Lau, C. Mattos, S. Michnick, T. Ngo, D.T. Nguyen, B. Prodhom, W.E. Reiher, B. Roux, M. Schlenkrich, J.C. Smith, R. Stote, J. Straub, M. Watanabe, J. Wiórkiewicz-Kuczera, D. Yin, M. Karplus, All-atom empirical potential for molecular modeling and dynamics studies of proteins, J. Phys. Chem. B 102 (1998) 3586–3616.
[37] A. Striolo, A.A. Chialvo, P.T. Cummings, K.E. Gubbins, Water adsorption in carbon-slit nanopores, Langmuir 19 (2003) 8583–8591.
[38] W.L. Jorgensen, J. Chandrasekhar, J.D. Madura, R.W. Impey, M.L. Klein, Comparison of simple potential functions for simulating liquid water, J. Chem. Phys. 79 (1983) 926–935.
[39] H.J.C. Berendsen, J.R. Grigera, T.P. Straatsma, The missing term in effective pair potentials, J. Phys. Chem. 91 (1987) 6269–6271.
[40] J.L.F. Abascal, C. Vega, A general purpose model for the condensed phases of water: TIP4P/2005, J. Chem. Phys. 123 (23) (2005) 234505, https://doi.org/10.1063/1.2121687.
[41] P. Florová, P. Sklenovský, P. Banáš, M. Otyepka, Explicit water models affect the specific solvation and dynamics of unfolded peptides while the conformational behavior and flexibility of folded peptides remain intact, J. Chem. Theory Comput. 6 (11) (2010) 3569–3579.
[42] F. Sajadi, C.N. Rowley, Simulations of lipid bilayers using the CHARMM36 force field with the TIP3P-FB and TIP4P-FB water models, PeerJ 6 (2018).
[43] C. Vega, J.L.F. Abascal, Simulating water with rigid non-polarizable models: a general perspective, PCCP 13 (44) (2011) 19663, https://doi.org/10.1039/c1cp22168j.
[44] R.H. Tunuguntla, R.Y. Henley, Y.-C. Yao, T.A. Pham, M. Wanunu, A. Noy, Enhanced water permeability and tunable ion selectivity in subnanometer carbon nanotube porins, Science 357 (6353) (2017) 792–796.
[45] Y.-C. Yao, A. Taqieddin, M.A. Alibakhshi, M. Wanunu, N.R. Aluru, A. Noy, Strong electroosmotic coupling dominates ion conductance of 1.5 nm diameter carbon nanotube porins, ACS Nano 13 (11) (2019) 12851–12859.
[46] M. Manghi, J. Palmeri, K. Yazda, F. Henn, V. Jourdain, Role of charge regulation and flow slip in the ionic conductance of nanopores: an analytical approach, Phys. Rev. E 98 (2018) 012605.

[47] M. Manghi, J. Palmeri, F. Henn, A. Noury, F. Picaud, G. Herlem, V. Jourdain, Ionic conductance of carbon nanotubes: confronting literature data with nanofluidic theory, J. Phys. Chem. C. https://doi.org/10.1021/acs.jpcc.1c08202(2021).
[48] R. Salih, C.C. Matthai, Computer simulations of the diffusion of Na+ and Cl− ions across POPC lipid bilayer membranes, J. Chem. Phys. 146 (2017) 105101.
[49] I.S. Joung, T.E. Cheatham, Molecular dynamics simulations of the dynamic and energetic properties of alkali and halide ions using water-model-specific ion parameters, J. Phys. Chem. B 113 (2009) 13279–13290.
[50] S. Buyukdagli, M. Manghi, J. Palmeri, Ionic capillary evaporation in weakly charged nanopores, Phys. Rev. Lett. 105 (2010) 158103.
[51] T. Hennequin, M. Manghi, J. Palmeri, Competition between Born solvation, dielectric exclusion, and Coulomb attraction in spherical nanopores, Phys. Rev. E 104 (4) (2021), https://doi.org/10.1103/PhysRevE.104.044601.
[52] V. Neklyudov, V. Freger, Water and ion transfer to narrow carbon nanotubes: roles of exterior and interior, J. Phys. Chem. Lett. 12 (2021) 185–190.
[53] M.H. Köhler, J.R. Bordin, C.F. de Matos, M.C. Barbosa, Water in nanotubes: the surface effect, Chem. Eng. Sci. 203 (2019) 54–67.
[54] M.H. Köhler, L.B. da Silva, Size effects and the role of density on the viscosity of water confined in carbon nanotubes, Chem. Phys. Lett. 645 (2016) 38–41.
[55] H. Kyakuno, M. Fukasawa, R. Ichimura, K. Matsuda, Y. Nakai, Y. Miyata, T. Saito, Y. Maniwa, Diameter-dependent hydrophobicity in carbon nanotubes, J. Chem. Phys. 145 (2016) 064514.
[56] S. Velioğlu, H.E. Karahan, K. Goh, T.-H. Bae, Y. Chen, J.W. Chew, Metallicity-dependent ultrafast water transport in carbon nanotubes, Small 16 (2020) 1907575.
[57] W. Song, M. Kumar, Artificial water channels: toward and beyond desalination, Curr. Opin. Chem. Eng. 25 (2019) 9–17.
[58] X. Wei, T. Luo, Effects of electrostatic interaction and chirality on the friction coefficient of water flow inside single-walled carbon nanotubes and boron nitride nanotubes, J. Phys. Chem. C 122 (2018) 5131–5140.
[59] L. Liu, G.N. Patey, Simulations of water transport through carbon nanotubes: How different water models influence the conduction rate, J. Chem. Phys. 141 (2014) 18C518.
[60] L. Liu, G.N. Patey, Simulated conduction rates of water through a (6,6) carbon nanotube strongly depend on bulk properties of the model employed, J. Chem. Phys. 144 (2016) 184502.
[61] L. Liu, G.N. Patey, A molecular dynamics investigation of the influence of water structure on ion conduction through a carbon nanotube, J. Chem. Phys. 146 (2017) 074502.
[62] S.H. Lee, J. Kim, Transport properties of bulk water at 243–550 K: a Comparative molecular dynamics simulation study using SPC/E, TIP4P, and TIP4P/2005 water models, Mol. Phys. 117 (2019) 1926–1933.
[63] A.T. Celebi, C.T. Nguyen, R. Hartkamp, A. Beskok, The role of water models on the prediction of slip length of water in graphene nanochannels, J. Chem. Phys. 151 (2019) 174705.
[64] J. Losey, S.K. Kannam, B.D. Todd, R.J. Sadus, Flow of water through carbon nanotubes predicted by different atomistic water models, J. Chem. Phys. 150 (2019) 194501.
[65] G.S. Fanourgakis, J.S. Medina, R. Prosmiti, Determining the bulk viscosity of rigid water models, J. Phys. Chem. A 116 (2012) 2564–2570.
[66] M.A. González, J.L.F. Abascal, The shear viscosity of rigid water models, J. Chem. Phys. 132 (2010) 096101.
[67] J. Dix, L. Lue, P. Carbone, Why different water models predict different structures under 2D confinement, J. Comput. Chem. 39 (2018) 2051–2059.